

Article

Research on the Anti-Reflective Cracking Performance of a Full-Depth Asphalt Pavement

Fujin Hou ¹, Tao Li ¹, Xu Li ², Yunliang Li ² and Meng Guo ^{3,*} 

¹ Shandong Hi-Speed Construction Management Group Co., Ltd., Jinan 250001, China; hfj7308@163.com (F.H.); lt1230823@163.com (T.L.)

² Harbin Institute of Technology, Harbin 150090, China; 15636100281@163.com (X.L.); liyl-hit@163.com (Y.L.)

³ The Key Laboratory of Urban Security and Disaster Engineering of Ministry of Education, Beijing University of Technology, Beijing 100124, China

* Correspondence: gm@bjut.edu.cn; Tel.: +86-18001205566

Abstract: In order to analyze the anti-reflective cracking performance of a full-depth asphalt pavement and study the propagation process of a reflection crack and its influencing factors, a mechanical model of pavement structural crack analysis was established based on the ABAQUS finite element software and the extended finite element method (XFEM). Based on two different loading modes of three-point bending and direct tension, the propagation process of a reflection crack is analyzed. The results show that the anti-reflective cracking performance of a full-depth asphalt pavement is better than that of a semi-rigid base pavement structure, and the loading mode II based on direct tension is more consistent with the propagation mechanism of pavement reflection cracks, while the loading mode I is more suitable for analyzing the anti-reflective cracking performance of the pavement structure. Appropriately reducing the elastic modulus of the stress-absorbing layer can significantly improve the anti-reflective cracking performance of the full-depth asphalt pavement.

Keywords: full-depth asphalt pavement; stress-absorbing layer; reflective cracking; extended finite element method



Citation: Hou, F.; Li, T.; Li, X.; Li, Y.; Guo, M. Research on the Anti-Reflective Cracking Performance of a Full-Depth Asphalt Pavement. *Sustainability* **2021**, *13*, 9499. <https://doi.org/10.3390/su13179499>

Academic Editor: Antonio D'Andrea

Received: 30 June 2021

Accepted: 11 August 2021

Published: 24 August 2021

Publisher's Note: MDPI stays neutral with regard to jurisdictional claims in published maps and institutional affiliations.



Copyright: © 2021 by the authors. Licensee MDPI, Basel, Switzerland. This article is an open access article distributed under the terms and conditions of the Creative Commons Attribution (CC BY) license (<https://creativecommons.org/licenses/by/4.0/>).

1. Introduction

Most of the asphalt pavement of high-grade highways in China adopts a semi-rigid base structure with enough strength and rigidity, good integrity, strong diffusion stress ability and good water stability, which can ensure the stability of the base [1–3]. But a semi-rigid base is prone to shrinkage crack and low temperature shrinkage crack [4–7]. Under the repeated action of the traffic load and temperature load, the asphalt surface layer tends to expand and form reflection cracks [8–11], which seriously affects the road's performance and shortens its life. At the same time, the performance of commonly used road cementing materials is greatly affected by the environment, and their mechanical properties are relatively complex, which further aggravates the occurrence of pavement crack disease [12–14]. As a kind of thick asphalt concrete pavement structure with a broad development prospect in recent years, the full-depth asphalt pavement [15–18] has unique advantages compared with other types of pavement, which are generally made of modified asphalt and recycled asphalt [19–21] as pavement asphalt materials. The full-depth asphalt pavement is not easily damaged, and the cracks have a small influence depth; no major structural repair is required, which saves costs; the road life is long, and the maintenance cost is reduced. More importantly, the full-depth asphalt pavement can effectively prevent and control reflection cracks.

As early as the 1960s, North America began to build full-depth and thickened asphalt pavement, and put forward the concepts of permanent pavement and long-life pavement. Donath M. Mrawira and Joseph Luca [22] studied the thermal and physical characteristics of full-depth asphalt pavement earlier and numerically analyzed the transient temperature

response by using the energy balance principle and a Fourier heat transfer equation. Halil Ceylan et al. [23] used the artificial neural network as the pavement structure analysis tool to calculate the modulus of full-depth asphalt pavement considering the nonlinear stress-dependent subgrade characteristics, and verified its accuracy; Pekcan O et al. [24] developed a calculation method called SOFTSYS, which can use the test results of a drop hammer deflection meter to calculate the performance of full-depth pavement structure layers, and check it with concrete examples. Emad Kassem et al. [25] evaluated the construction of a full-depth asphalt pavement by using X-ray computed tomography and ground-penetrating radar technology. Some scholars have also studied the performance and response of recycled full-depth asphalt pavement [26]. Compared with traditional maintenance methods, this method has advantages in the cost and life cycle [27].

The main advantage of a full-depth asphalt pavement is its good cracking resistance. At present, many scholars have simulated the cracking process of asphalt pavement. Seong Hyeok Song et al. [28] developed a cohesive regional model using the finite element software ABAQUS, and simulated the mixed-mode cracks' propagation process of a single-edge notched beam test using the calibrated cohesion parameters. The results were compared with the experimental results, which proved that the crack trajectory predicted by the numerical simulation was in good agreement with the experimental results. Yekai Chen and Jinchang Wang [29] used the extended finite element method (XFEM) to simulate the crack propagation process of asphalt concrete and successfully predicted the low temperature cracking behavior of an asphalt pavement. Aiming at the problem of early cracks in asphalt pavement, Zhong Yanhui et al. [30] conducted a three-dimensional numerical simulation of an asphalt pavement with ABAQUS, based on the fracture mechanics theory, and analyzed the corresponding and propagation characteristics of cracks in an asphalt pavement under moving loads. Sang Luo et al. [31] established the finite element model of crack propagation of an epoxy asphalt concrete pavement and carried out the numerical simulation combined with the virtual crack extension approach. They analyzed the cracking process by stages and provided the equation describing the relationship between the J-integral and displacement. According to the basic theory of fracture mechanics and the finite element model, Hongbing Guo and Shuanfa Chen [32] simulated the propagation path of a reflection crack on an Open-graded Large Stone asphalt Mix (OLSM) pavement, analyzed the influencing factors of the path and proposed a method to prolong the life of this pavement. Xiaochun Zhang et al. [33] established a three-dimensional finite element model of an asphalt pavement's hydraulic crack, analyzed its propagation process under vehicle load and discussed the influence of various parameters on the crack. Shangyang Yang used [34] the finite element method to simulate a semi-rigid asphalt pavement under temperature change and studied the influence of some parameters on the stress intensity factor. Pengfei Liu et al. [35] applied the Cohesion Zone Model (CZM) approach to ABAQUS to analyze crack propagation in asphalt layers. The results show that the developed CZM approach can effectively supplement the traditional design method and improve the computational efficiency and accuracy.

In addition to the full-depth asphalt pavement, the use of a stress-absorbing layer [36–39] can also prevent the base reflection crack disease. At present, the materials commonly used for the stress-absorbing layer of an asphalt pavement include a warm mix rubber modified asphalt mixture [40,41], the intelligent composite materials [42] and geosynthetics [43] such as fabrics, grids and composites. These materials have proved to be able to improve the cracking resistance of pavement structures. However, in the numerical simulation, the difference between the stress-absorption layer and other structural layers can only be characterized by changing some parameters.

It can be seen that great progress has been made in the simulation of asphalt pavement cracks, but there is no relevant simulation for the crack propagation process of a full-depth asphalt pavement. Therefore, the simulation research on this aspect is very necessary. In this paper, based on the ABAQUS finite element software, the extended finite element method (XFEM) is used to analyze the anti-reflective cracking performance of a full-depth

asphalt pavement. This paper analyzes the formation and propagation process of reflection cracks in a full-depth asphalt pavement and studies the influencing factors of the anti-reflective cracking performance of a full-depth asphalt pavement. The influence of different pavement structure types on anti-reflective cracking performance is compared. At the same time, the effect of the modulus of the stress-absorbing layer on the cracking resistance of the structure is studied. This paper has a guiding significance for the selection of full-depth asphalt pavement structures and the mix design of the stress-absorbing layer.

2. Reflection Crack Analysis Model of a Full-Depth Asphalt Pavement

2.1. Full-Depth Asphalt Pavement Structure

In order to analyze the influence of a pavement's structure on its anti-reflective cracking performance and to compare and analyze the difference of anti-reflective cracking performance between a full-depth asphalt pavement and a general semi-rigid base asphalt pavement, five different pavement structure types are selected, as shown in Figure 1. Structures I, II and III refer to a full-depth asphalt pavement, and structures IV and V refer to a general semi-rigid base asphalt pavement. The thickness and material of each layer of the five pavement structures are shown in Figure 1, and the material parameters are shown in Table 1.

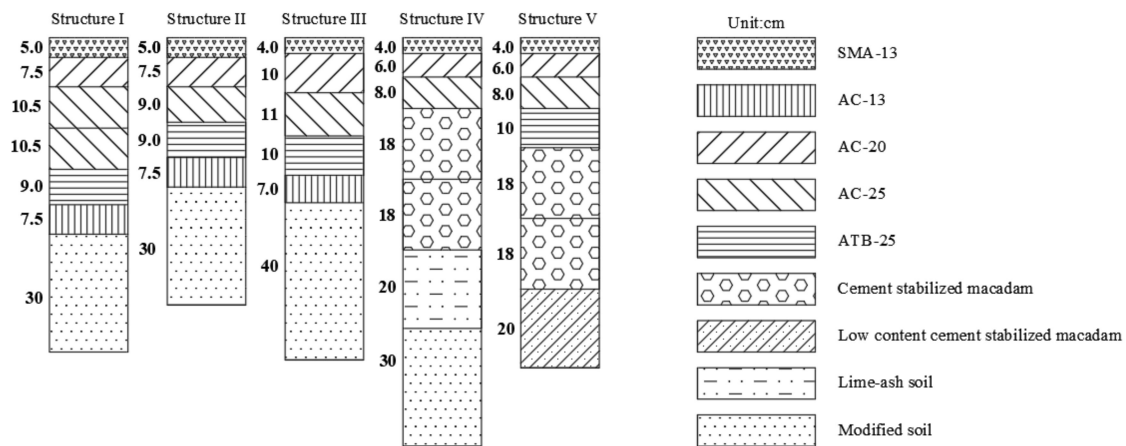


Figure 1. Pavement structure and materials.

Table 1. Relevant parameters of various pavement materials.

Material Name	Elastic Modulus (MPa)	Poisson's Ratio
SMA-13	1500	0.25
AC-13	1450	0.25
AC-20	1400	0.25
AC-25	1350	0.25
ATB-25	1200	0.40
Lime-ash soil	800	0.35
Cement stabilized macadam	1600	0.25
Low content cement stabilized macadam	1300	0.25
Modified soil	400	0.40
Soil	50	0.40

In the numerical simulation, the different materials are mainly reflected by the different parameters. Cement stabilized macadam is a semi-rigid material, so its elastic modulus is larger and its Poisson's ratio is smaller. For several asphalt mixtures, there is little difference in the use of modulus values. In order to distinguish them, some adjustments have been made to the value.

2.2. Numerical Analysis Model

According to the above pavement structure scheme, the mechanical model of cracking analysis is established. The width of the model is 2 m, the thickness of the cement stabilized macadam layer of the five pavement structures is 10 cm and the total thickness is 60 cm, 48 cm, 52 cm, 64 cm and 38 cm, respectively. In order to analyze the cracking process of reflection cracks, two different loading modes are adopted.

Loading mode I: Analytical model based on the three-point bending mode. Supports are placed on the left and right sides of the lower part of the model, and the distance between the supports is 1800 mm. A indenter is set in the middle of the top of the model to apply the load downward. The indenter and supports are defined as analytical rigid bodies with infinite stiffness. The displacement is 6 mm by applying a vertical downward displacement at the indenter position. Prefabricated cracks are set in the middle of the cement stabilized macadam layer 10 cm below the model. Loading mode I is shown in Figure 2.

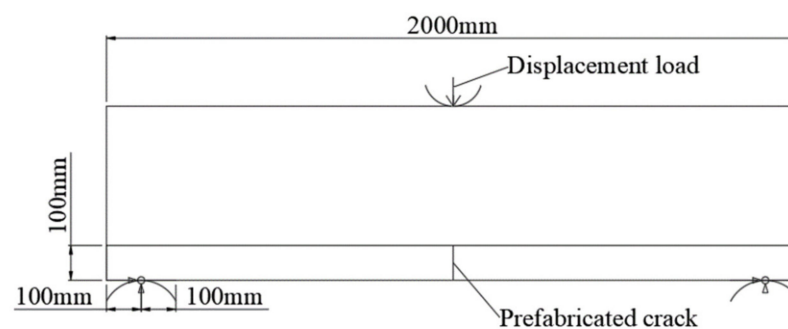


Figure 2. Loading mode I.

Loading mode II: Analytical model based on the direct tension mode. The lower side of the model is a free boundary, and the boundary conditions are set on the left and right sides of the bottom cement stabilized macadam layer. The left side is completely fixed, the right side is fixed with vertical displacement and the transverse tensile displacement is 1 mm. Prefabricated cracks are set in the middle of the cement stabilized macadam layer 10 cm below the model. Loading mode II is shown in Figure 3.

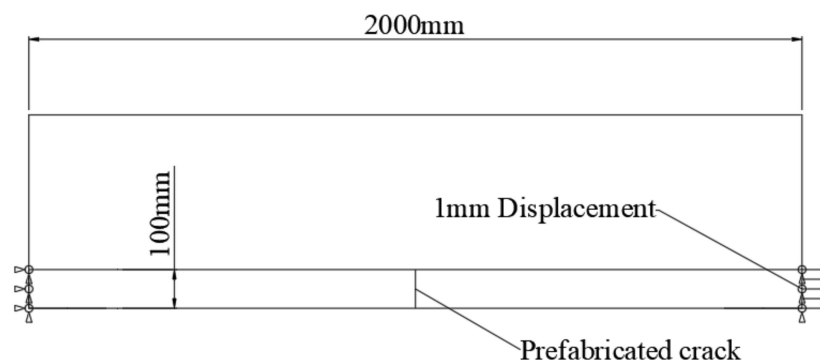


Figure 3. Loading mode II.

The extended finite element method (XFEM) is used to establish the finite element model. The CPS4R element—namely, the four-node bilinear plane stress quadrilateral element—is used as the mesh. The vertical side length of the mesh is 10 mm, and the finite element model is shown in Figure 4. It is assumed that the pavement material is homogeneous and isotropic, and the layers are completely continuous.

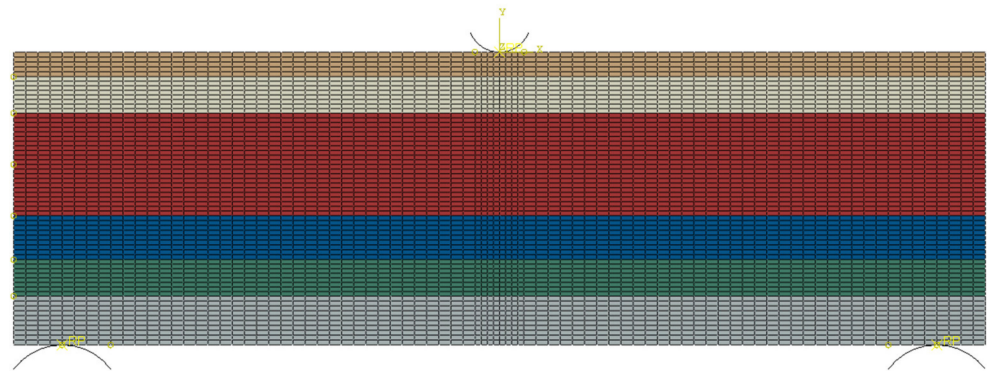
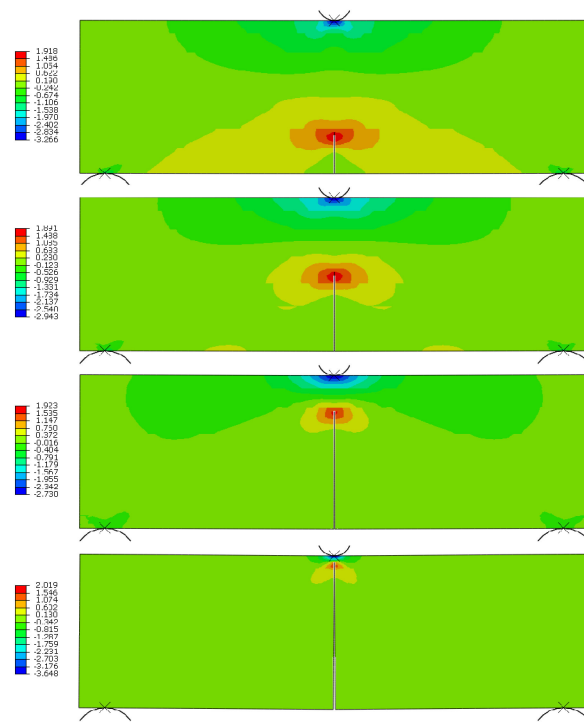


Figure 4. Finite element model for crack analysis.

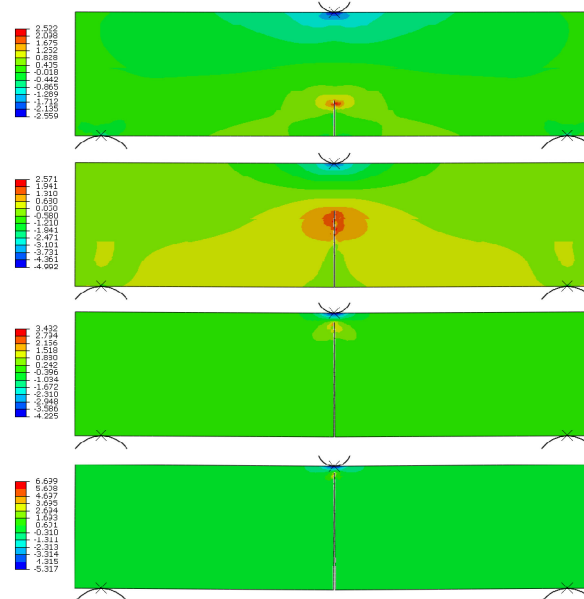
3. Analysis and Discussion

3.1. Reflection Crack Propagation Process

At present, there is no relevant research on the numerical simulation of the anti-reflective cracking performance of a full-depth asphalt pavement. By comparing the research results of this paper with similar references [44], the crack propagation path is the same, which preliminarily proves the correctness of this research method. Based on loading mode I, the propagation process of reflection cracks in five pavement structures is obtained. When the loading displacement of the indenter on the model is 1.5 mm, 3 mm, 4.5 mm and 6 mm, respectively, the transverse stress nephogram of the five pavement structures is shown in Figure 5. It can be seen from Figure 5 that the cracking process of different pavement structures is basically the same. During the whole cracking process, the stress is concentrated at the crack tip and the upper part of the structure, and the absolute value of the stress at the contact point of the indenter is larger, while the stress at the lower support is smaller, and thus closer to the other parts of the structure. At the initial stage of loading, the stress at the indenter diffuses to all sides, and the stress at the crack tip diffuses to the left and right oblique downward. When the displacement load is half loaded, the stress at the bottom of the crack tip decreases and the crack propagation speed increases. When the displacement load increases from 3 mm to 4.5 mm, the crack expands rapidly, and the stress concentration range at the crack tip shrinks and becomes oblate. Because the crack tip is close to the upper load application position, the stress diffusion area at the indenter to the left and right sides increases, and the diffusion range to the lower side decreases. Finally, when the displacement load is fully applied, the crack expands to the loading point, the stress area at the crack tip is in the shape of an inverted heart and the stress is concentrated at the crack tip and the indenter. The stress in other parts of the structure is small and evenly distributed.

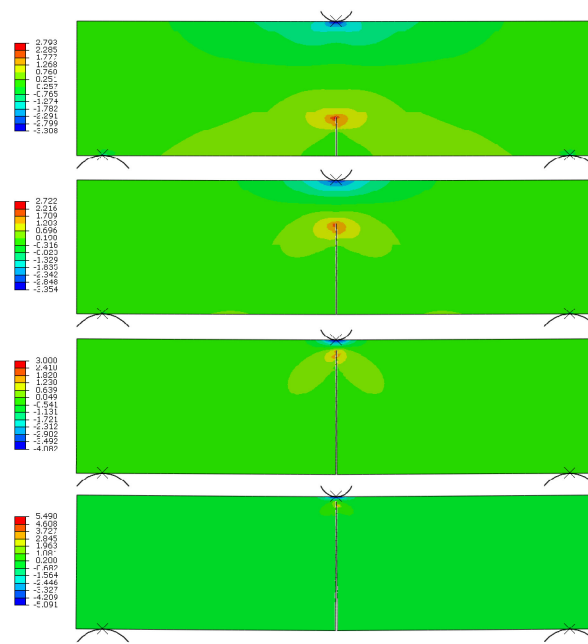


(a) Structure I transverse stress nephogram

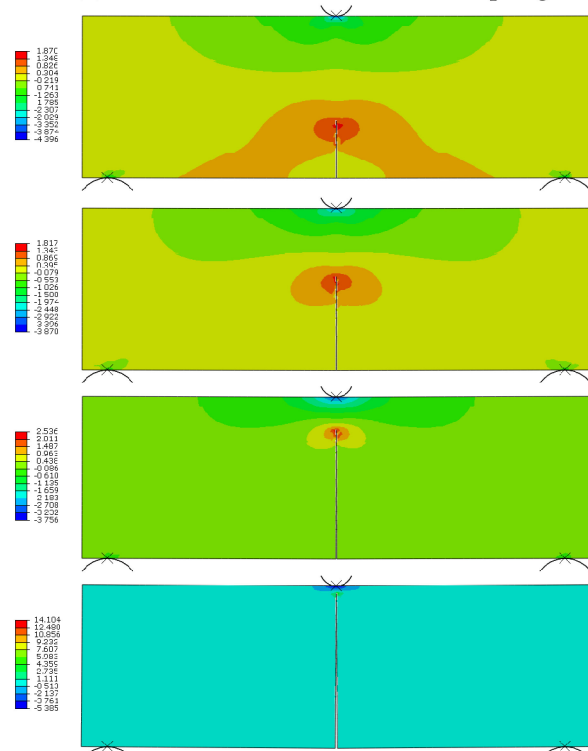


(b) Structure II transverse stress nephogram

Figure 5. Cont.



(c) Structure III transverse stress nephogram



(d) Structure IV transverse stress nephogram

Figure 5. Cont.

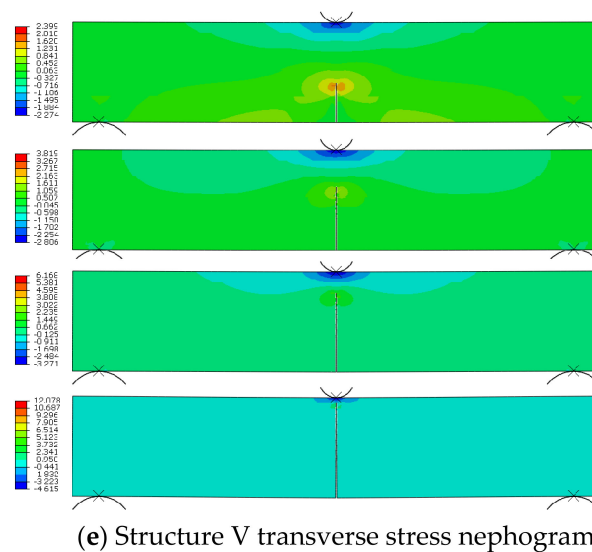


Figure 5. Propagation of a reflection crack in a pavement structure.

3.2. Load-Displacement Curve

The cracking process of five pavement structures is obtained based on loading mode I. Through further analysis, the vertical displacement of the contact position between the indenter and the model can be obtained, and then the load-displacement curves of five pavement structures can be obtained. Based on the load displacement curve, the anti-reflective crack performance of different pavement structures can be analyzed. The load-displacement curves of five pavement structures are shown in Figure 6. It can be seen from Figure 6 that the trend of load-displacement curves of different pavement structures is basically the same.

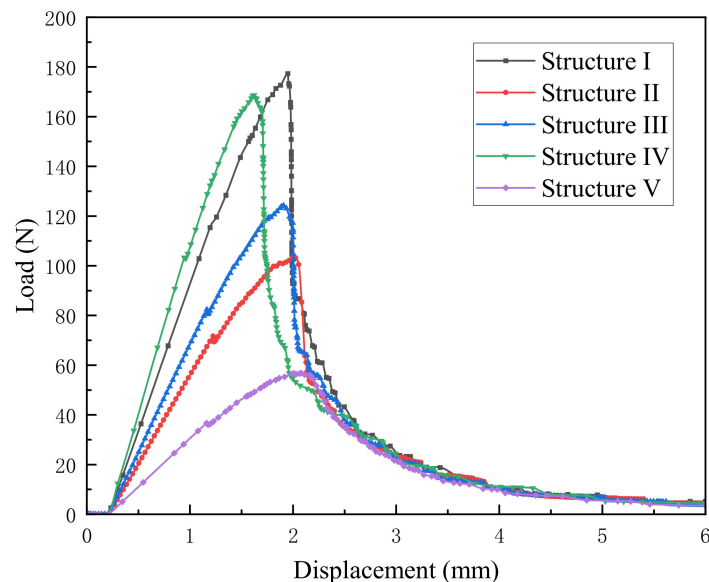


Figure 6. Load-displacement curves of five structures.

According to the variation law of the load-displacement curve, the fracture process of the structure can be divided into three stages. The first stage is the complete elastic stage, in which the load increases linearly with the increase of displacement and the growth rate of the five structures is different. At this stage, the curve is similar to the elastic deformation stage, when the crack growth rate is slow. The curves of the five structures reach the peak value when the displacement reaches about 2 mm, and then the load decreases rapidly

with the increase of displacement, entering the stage of crack initiation and the propagation stage. At this stage, there are some differences in the curves of the five structures: the load of the other four structures, except for structure V, is reduced by nearly half, while the load of structure V is decreased gently. At this time, the crack propagation rate is faster and the structure cracks rapidly. Finally, with the increase of displacement, the structure enters the complete fracture stage, in which the load is small and the curves of the five structures roughly coincide. The whole structure is nearly destroyed, but not completely cracked.

Although the forms of the load-displacement curves of different pavement structures are basically the same, the corresponding displacements and load peaks of the five pavement structures are different when the load reaches the maximum. When the different pavement structure curves reach the peak, the corresponding displacement is between 1.5 mm~2.2 mm, and the difference is not very big. The maximum load values of the five pavement structures are 177.33 n, 103.20 n, 124.24 n, 168.67 n and 56.81 n, respectively. The distance between the two supports under the model is 1800 mm. It can be seen that the maximum load value of the model is relatively small, which is due to the large distance between the supports of the model. However, from the relative value of the maximum load, the anti-cracking performance of structure I is the best, followed by structure IV, structure III and structure II, and structure V is the worst.

3.3. Contrastive Analysis of Fracture Parameters

Loading mode II is different from loading mode I in the crack propagation mechanism. The crack propagation of loading mode I is driven by road load, which is different from the mechanism of reflection crack. Reflection crack is the upward expansion of the crack caused by the tensile effect of the deformation of the underlying material after the cracking of the pavement's bottom layer. Based on this point, loading mode II can better analyze the formation process of reflection cracks and the anti-reflective cracking performance of different pavement structures.

In the simulation analysis of loading mode II, the output parameter PHILSM is the specified displacement function describing the crack surface, namely the hierarchical set value, which can be understood as displaying the contour surface of the crack. When the crack passes through an element, the value of PHILSM will appear on all four nodes of the element. The PHILSM value of the node on the same side of the crack is the same. The position where the value of PHILSM between nodes is 0 is the point where the crack passes through the element. Therefore, the length of the crack can be determined by the position of the crack (excluding the length of the prefabricated crack) in the output PHILSM nephogram, and the width of the crack can be determined by the lateral displacement of the left and right elements at the specified position. Figure 7 shows the nephogram of PHILSM at the cracking location of structure I, which has been enlarged. As shown in Figure 7, the gray part is the area without the PHILSM value, while the colored part has the PHILSM value, that is, the cracking position. As can be seen from the caption, the part where the value is 0 is orange, so the location of the crack can be more intuitively determined, and the crack's length and width can be obtained.

Based on the analysis of loading mode II, when the lateral loading displacement is 1 mm, the comparison of the width and length of the cracks in the different pavement structures is shown in Figure 8. Under this loading mode, the crack widths generated by the five structures are 0.1107 mm, 0.1323 mm, 0.1236 mm, 0.1569 mm and 0.7142 mm, respectively, and the crack lengths are 30 mm, 37.5 mm, 35 mm, 63 mm and 50 mm, respectively. It can be seen from Figure 8. that the length and width of the cracks in pavement structures I, II and III are relatively close, and they are smaller than those of pavement structure IV and pavement structure V. The crack width of pavement structure V is the largest, while the crack length of structure IV is the largest. It can be seen that the anti-reflective cracking performance of a full-depth asphalt pavement structure is better than that of a general semi-rigid base pavement structure, and through the comparative analysis of loading mode I and loading mode II, it can be seen that loading mode II is the

direct tensile loading mode, which can better simulate the cracking process of reflection cracks. Compared with the commonly used three-point bending loading mode I, loading mode II is more suitable for analyzing the propagation process of reflection cracks, and it is more suitable to analyze the anti-reflective cracking performance of a pavement structure.

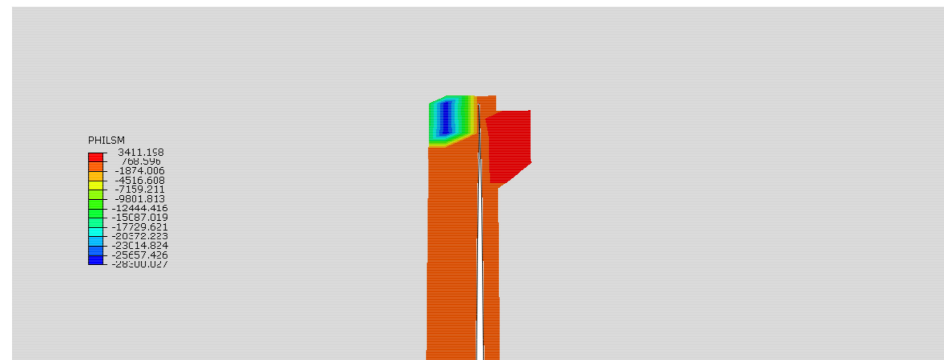


Figure 7. PHILSM nephogram (Structure I).

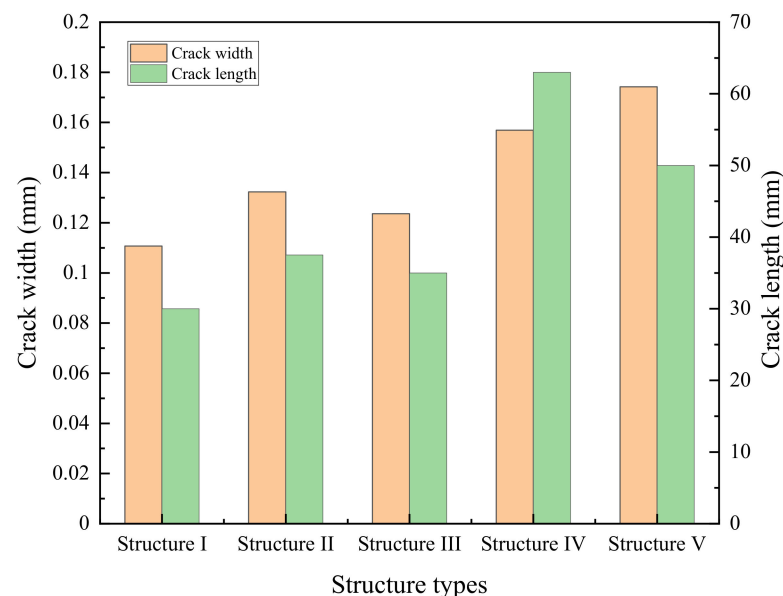


Figure 8. Crack length and width of five pavement structures.

3.4. Influence Analysis of Material Parameters

In the actual pavement structure, in order to improve the ability of anti-reflective cracks, a stress-absorbing layer is set in the lower layer of the pavement structure to delay the expansion of reflection cracks to the pavement structure layer through the deformation of the stress-absorbing layer. The above analysis shows that pavement structure I has the best anti-reflective cracking performance among the five pavement structure types. In pavement structure I, the upper layer of the precast crack is AC-13. The material properties of this layer have a great influence on the upward propagation of the precast crack, which is equivalent to that of the stress-absorbing layer. Through the reasonable setting of the material properties of this layer, the upward propagation of the crack can be delayed.

In order to analyze the influence of the stress-absorbing layer on pavement structure cracking, in pavement structure I, the elastic modulus of the stress-absorbing layer is changed by controlling the variable method, and the values of the elastic modulus are 1000 MPa, 1200 MPa, 1400 MPa, 1600 MPa, 1800 MPa and 2000 MPa, respectively. The influence of the material parameters on the reflection crack's propagation is analyzed.

Based on loading mode I, the load-displacement curves of pavement structure I under different elastic modulus are obtained, as shown in Figure 9. It can be seen from Figure 9 that the elastic modulus of the stress-absorbing layer has a certain influence on the load-displacement curve of the structure. The larger the elastic modulus, the larger the slope of the curve at the initial stage of loading, and the smaller the load peak that can be reached. Therefore, when considering the use of a stress-absorbing layer, a material with a lower elastic modulus can effectively improve the cracking resistance of the pavement structure.

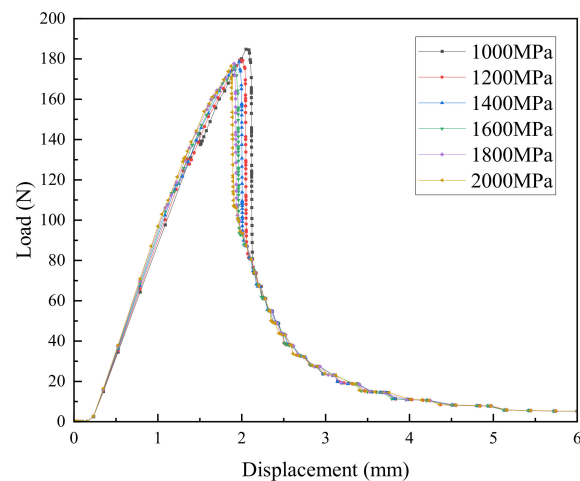


Figure 9. Influence of the modulus of the stress-absorbing layer on the load-displacement curve.

Based on loading mode II, the anti-cracking performance of pavement structure I under the change of the modulus of the stress-absorbing layer can be further analyzed. Under loading mode II, the change of the crack's width and length with the elastic modulus is shown in Figure 10. As can be seen from Figure 10, when the elastic modulus of the stress-absorbing layer varies between 1000 MPa and 2000 MPa, the crack width varies little. With the increase of the elastic modulus, the crack width is basically unchanged at the beginning, and then slightly increases. However, the fracture length undergoes an obvious variation with the elastic modulus of the stress-absorbing layer. The larger the elastic modulus, the larger the corresponding crack length. This is consistent with the conclusion based on the analysis of loading mode I, according to which the anti-cracking performance of pavement structure can be enhanced by reducing the elastic modulus of the stress-absorbing layer.

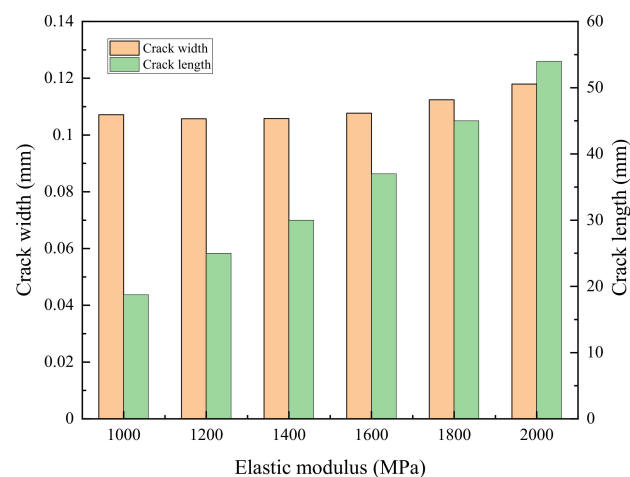


Figure 10. The influence of the modulus of the stress-absorbing layer on the fracture parameters.

4. Conclusions

Based on the above analysis, the following conclusions can be drawn.

(1) Based on the mechanism of reflection cracks in a full-depth pavement structure, two different analysis models are established. Based on the three-point bending loading mode and the direct tensile loading mode, five mechanical models for the cracking analysis of different pavement structures were established, respectively.

(2) The stress distribution characteristics and crack propagation process of the pavement cracking process are analyzed. The anti-cracking performance of different pavement structures is studied. During the whole cracking process, the stress is concentrated at the crack tip, and the crack propagation of the pavement structure includes three stages: complete elastic stage, crack initiation and propagation stage, and complete fracture stage. The crack resistance of the pavement structure can be improved by using the full-depth pavement structure.

(3) Loading mode II, under a direct tensile condition, can better simulate the cracking process of reflection cracks. Compared with three-point bending loading mode I, loading mode II is more suitable for analyzing the expansion process of reflective cracks and the anti-reflective cracking performance of the pavement structure.

(4) The crack length varies obviously with the elastic modulus of the stress-absorbing layer. The larger the elastic modulus, the longer the corresponding reflection crack. By setting the stress-absorbing layer and appropriately reducing the elastic modulus of the stress-absorbing layer, the anti-reflective cracking performance of the pavement structure can be significantly improved.

Author Contributions: Data curation, T.L.; investigation, X.L.; methodology, M.G.; project administration, F.H.; supervision, Y.L. All authors have read and agreed to the published version of the manuscript.

Funding: This study was supported by the National Natural Science Foundation of China (51808016, 52078018), the Young Elite Scientists Sponsorship Program of China's Association for Science and Technology (2018QNRC001) and Transportation Science and Technology Project of Shandong Province (2020B25).

Institutional Review Board Statement: Not applicable.

Informed Consent Statement: Not applicable.

Data Availability Statement: The data presented in this study are available in this manuscript.

Conflicts of Interest: The authors declare no conflict of interest.

References

1. Sun, Z.-H.; Ma, J.; Su, X.-M.; Yang, G.-F.; Hou, Z.-Q. Grey Relational Analysis of Fatigue Performance of Semi-Rigid Pavement Structure. *Appl. Mech. Mater.* **2014**, *651–653*, 1164–1167. [[CrossRef](#)]
2. Wang, Y.-Q.; Tan, Y.-Q.; Guo, M.; Liu, Z.-Y.; Wang, X.-L. Study on the dynamic compressive resilient modulus and frost resistance of semi-rigid base materials. *Road Mater. Pavement Des.* **2017**, *18*, 259–269. [[CrossRef](#)]
3. Dong, Q.; Zhao, X.-K.; Chen, X.-Q.; Ma, X.; Cui, X.-Q. Long-term mechanical properties of in situ semi-rigid base materials. *Road Mater. Pavement Des.* **2021**, *22*, 1692–1707. [[CrossRef](#)]
4. Zhang, P.; Li, Q.-F.; Liu, C.-H. Prediction of shrinkage cracking and corresponding cracking prevention measure of the semi-rigid base layer. *Int. J. Pavement Eng.* **2009**, *10*, 383–388.
5. Yu, S.-X.; Wei, J.-C.; Li, X.-W.; Ma, S.-J. Shrinkage Characteristics of Cement Treated Base Subjected to Thermal Coupled with Moisture in the Field. *Appl. Mech. Mater.* **2013**, *361–363*, 1621–1624. [[CrossRef](#)]
6. Su, L.-Y. Mechanics Analysis of Semi-Rigid Subgrade Pavement Structure. *Appl. Mech. Mater.* **2014**, *580–583*, 105–108. [[CrossRef](#)]
7. Zang, G.-S.; Sun, L.-J.; Chen, Z.; Li, L. A nondestructive evaluation method for semi-rigid base cracking condition of asphalt pavement. *Constr. Build. Mater.* **2018**, *162*, 892–897. [[CrossRef](#)]
8. Livneh, M.; Ishai, I.; Kief, O. Bituminous pre-coated geotextile felts for retarding reflection cracks. *Reflective Crack. Pavements* **1993**, *20*, 343–350.
9. Doh, Y.S.; Baek, S.H.; Kim, K.W. Estimation of relative performance of reinforced overlaid asphalt concretes against reflection cracking due to bending more fracture. *Constr. Build. Mater.* **2009**, *23*, 1803–1807. [[CrossRef](#)]

10. Wang, X.-Y.; Zhong, Y. Reflective crack in semi-rigid base asphalt pavement under temperature-traffic coupled dynamics using XFEM. *Constr. Build. Mater.* **2019**, *214*, 280–289. [[CrossRef](#)]
11. Gao, Y.-Y. Theoretical Analysis of Reflective Cracking in Asphalt Pavement with Semi-rigid Base. *Iran. J. Sci. Technol. Trans. Civ. Eng.* **2019**, *43*, 149–157. [[CrossRef](#)]
12. Thom, N.; Dawson, A. Sustainable Road Design: Promoting Recycling and Non-Conventional Materials. *Sustainability* **2019**, *11*, 21. [[CrossRef](#)]
13. Cheraghian, G.; Wistuba, M.P. Ultraviolet aging study on bitumen modified by a composite of clay and fumed silica nanoparticles. *Nature* **2020**, *10*, 11216.
14. Cheraghian, G.; Wistuba, M.P.; Kiani, S.; Barron, A.; Behnood, A. Rheological, physicochemical, and microstructural properties of asphalt binder modified by fumed silica nanoparticles. *Sci. Rep.* **2021**, *11*, 11455. [[CrossRef](#)] [[PubMed](#)]
15. Linear tracking performance tests on full-depth asphalt pavement. *Transp. Res. Rec. J. Transp. Res. Board* **1997**, *1570*, 39–47. [[CrossRef](#)]
16. Lane, B.; Kazmierowski, T. Ten-Year Performance of Full-Depth Reclamation with Expanded Asphalt Stabilization on Trans-Canada Highway, Ontario, Canada. *Transp. Res. Rec.* **2012**, *2306*, 45–51. [[CrossRef](#)]
17. Dessouky, S.H.; Al-Qadi, I.L.; Yoo, P.J. Full-depth flexible pavement responses to different truck tyre geometry configurations. *Int. J. Pavement Eng.* **2014**, *15*, 512–520. [[CrossRef](#)]
18. Melese, E.; Baaj, H.; Tighe, S.; Zupko, S.; Smith, T. Characterisation of full-depth reclaimed pavement materials treated with hydraulic road binders. *Constr. Build. Mater.* **2019**, *226*, 778–792. [[CrossRef](#)]
19. Guo, M.; Liu, H.-Q.; Jiao, Y.-B.; Mo, L.-T.; Tan, Y.-Q.; Wang, D.-W.; Liang, M.-C. Effect of WMA-RAP Technology on Pavement Performance of Asphalt Mixture: A State-of-the-Art Review. *J. Clean. Prod.* **2020**, *266*, 121704. [[CrossRef](#)]
20. Guo, M.; Liu, X.; Jiao, Y.-B.; Tan, Y.-Q.; Luo, D.-S. Rheological characterization of reversibility between aging and rejuvenation of common modified asphalt binders. *Constr. Build. Mater.* **2021**, *301*, 124077. [[CrossRef](#)]
21. Guo, M.; Liang, M.-C.; Sreeram, A.; Bhasin, A.; Luo, D.-S. Characterization of Rejuvenation of Various Modified Asphalt Binders based on Simplified Chromatographic Techniques. *Int. J. Pavement Eng.* **2021**. [[CrossRef](#)]
22. Mrawira, D.M.; Luca, J. Thermal Properties and Transient Temperature Response of Full-Depth Asphalt Pavements. *Transp. Res. Rec.* **2002**, *1809*, 160–171. [[CrossRef](#)]
23. Ceylan, H.; Guclu, A.; Tutumluer, E.; Thompson, M.R. Backcalculation of full-depth asphalt pavement layer moduli considering nonlinear stress-dependent subgrade behavior. *Int. J. Pavement Eng.* **2005**, *6*, 171–182. [[CrossRef](#)]
24. Pekcan, O.; Tutumluer, E.; Ghaboussi, J. SOFTSYS for Backcalculation of Full-Depth Asphalt Pavement Layer Moduli. In Proceedings of the 8th International Conference on the Bearing Capacity of Roads, Railways and Airfields, Champaign, IL, USA, 29 June–2 July 2009; pp. 679–687.
25. Kassem, E.; Walubita, L.; Scullion, T.; Masad, E.; Wimsatt, A. Evaluation of Full-Depth Asphalt Pavement Construction Using X-Ray Computed Tomography and Ground Penetrating Radar. *J. Perform. Constr. Facil.* **2008**, *22*, 408–416. [[CrossRef](#)]
26. Johanneck, L.; Dai, S.-T. Responses and Performance of Stabilized Full-Depth Reclaimed Pavements at the Minnesota Road Research Facility. *Transp. Res. Rec.* **2013**, *2368*, 114–125. [[CrossRef](#)]
27. Braham, A. Comparing Life-Cycle Cost Analysis of Full-Depth Reclamation Versus Traditional Pavement Maintenance and Rehabilitation Strategies. *Transp. Res. Rec.* **2016**, *2573*, 49–59. [[CrossRef](#)]
28. Song, S.H.; Paulino, G.H.; Buttlar, W.G. Simulation of Crack Propagation in Asphalt Concrete Using an Intrinsic Cohesive Zone Model. *J. Eng. Mech.* **2006**, *132*, 1215–1223. [[CrossRef](#)]
29. Chen, Y.-K.; Wang, J.-C. Simulation of Crack Propagation in Asphalt Concrete Pavement at Low Temperature Using Extended Finite Element Method. In Proceedings of the International Workshop on Energy and Environment in the Development of Sustainable Asphalt Pavements, Xi'an, China, 6–8 June 2010.
30. Zhong, Y.-H.; Zhang, B.; Zhong, Y.-M.; Guo, C.-C. Response Analysis of Surface Crack in Asphalt Pavement under Moving Loads. *Adv. Mater. Res.* **2011**, *250–253*, 2769–2772. [[CrossRef](#)]
31. Luo, S.; Qian, Z.-D.; Chen, C. Crack Propagation Simulation for Epoxy Asphalt Concrete Pavement. *Key Eng. Mater.* **2011**, *460–461*, 698–703. [[CrossRef](#)]
32. Guo, H.-B.; Chen, S.-F. Numerical Simulation of the Reflective Crack Propagation Path for Open-Graded Large Stone Asphalt Mixes. *J. Wuhan Univ. Technol.* **2010**, *152–153*, 180–183. [[CrossRef](#)]
33. Zhang, X.-C.; Sun, F.-M.; Wang, Y.; Zhang, N. Fracture Mechanics Analysis of Hydraulic Cracks in Asphalt Pavement. *Appl. Mech. Mater.* **2012**, *138–139*, 478–483. [[CrossRef](#)]
34. Yang, S.-Y. Finite Element Transient Analysis on the Highway Reflective Crack in Temperature Change. *Adv. Mater. Res.* **2012**, *594–597*, 1482–1485. [[CrossRef](#)]
35. Liu, P.-F.; Chen, J.; Lu, G.-Y.; Wang, D.-W.; Oeser, M.; Leischner, S. Numerical Simulation of Crack Propagation in Flexible Asphalt Pavements Based on Cohesive Zone Model Developed from Asphalt Mixtures. *Materials* **2019**, *12*, 1278. [[CrossRef](#)] [[PubMed](#)]
36. Dempsey, B. Development and Performance of Interlayer Stress-Absorbing Composite in Asphalt Concrete Overlays. *Transp. Res. Rec. J. Transp. Res. Board* **2002**, *1809*, 175–183. [[CrossRef](#)]
37. Cao, W.-D.; Yao, Z.-Y.; Shang, Q.-S.; Li, Y.-Y.; Yang, Y.-S. Performance Evaluation of Large Stone Porous Asphalt-Rubber Mixture. *Adv. Mater. Res.* **2011**, *150–151*, 1184–1190. [[CrossRef](#)]

38. Liu, J.-Y.; Zhang, L.-J.; Kou, B.; Shen, P. The Environment-Friendly High-Elasticity Asphalt Mixture Using as Stress Absorbing Layer. *Adv. Mater. Res.* **2012**, *490–495*, 3753–3761. [[CrossRef](#)]
39. Baek, C. Performance Evaluation of Fiber-Reinforced, Stress Relief Asphalt Layers to Suppress Reflective Cracks. *Appl. Sci.* **2020**, *10*, 7701. [[CrossRef](#)]
40. Tan, J.-Z.; Wei, J.-G.; Pan, C.; Huang, K.-X. Shear stress calculation of rubber asphalt overlay and stress-absorbing layer. In Proceedings of the 2016 International Conference on Civil, Architecture and Environmental Engineering, Taipei, Taiwan, 4–6 November 2016; CRC Press/Balkema: Boca Raton, FL, USA, 2016; Volume 1, pp. 189–193.
41. Pan, R.; Li, Y.-M. Effect of warm mix rubber modified asphalt mixture as stress absorbing layer on anti-crack performance in cold region. *Constr. Build. Mater.* **2020**, *251*, 118985. [[CrossRef](#)]
42. Deng, H.-L.; Fu, X.-Y.; Gao, W.-X.; Ni, T.-T.; Chen, K.-J. Research on New Technology to Control Highway Semi-Rigid Base Asphalt Pavement Cracks. *Adv. Mater. Res.* **2011**, *194–196*, 1632–1638. [[CrossRef](#)]
43. Wargo, A.; Safavizadeh, S.A.; Kim, Y.R. Comparing the Performance of Fiberglass Grid with Composite Interlayer Systems in Asphalt Concrete. *Transp. Res. Rec.* **2017**, *2631*, 123–132. [[CrossRef](#)]
44. Li, P.; Mao, Y.; Nian, T.-F.; Ma, K. Crack propagation behavior between base and surface courses of asphalt pavement based on weight function method. *J. Beijing Jiaotong Univ.* **2017**, *41*, 61–68. (In Chinese)